Status of Mars Retropropulsion Testing in the Langley Unitary Plan Wind Tunnel

Karl T. Edquist*

NASA Langley Research Center, Hampton, Virginia 23681

Future Mars human landings will be enabled by a powered descent phase starting at supersonic conditions, something which has never been done before on a Mars mission. Significant aerosciences challenges exist due to jet interactions between the retrorocket engine plumes, freestream flow, and vehicle that will affect the aerodynamic behavior during powered descent. Historically, wind tunnel tests have been used to study the interactions with inert gas exhaust simulants in place of rocket engines. On the computational side, flowfield simulations have been completed at full-scale conditions, but the available ground and flight data are not appropriate for calibrating computational uncertainties for aerodynamic interference on proposed Mars descent vehicles, due to insufficient data, dissimilar vehicle geometries, and disparate operating conditions. A wind tunnel test has been designed to begin addressing powered descent aerodynamics risks for large-scale human Mars entry concepts and to identify gaps in computational predictive capabilities. The test will be conducted in the NASA Langley Unitary Plan Wind Tunnel and is designed with improvements in model design and data products over past tests. The test campaign will be run using sub-scale model geometries derived from NASA powered descent reference vehicles: a blunt low lift-to-drag vehicle and a more slender geometry that generates higher unpowered lift. Both models have been fabricated and are ready for testing. The blunt model is equipped with the flexibility to examine the effects of nozzle pointing direction, number, location, size, and area ratio. The main measurements are heatshield aerodynamic interference forces and moments with a custom flow-through balance, discrete and distributed heatshield pressure, and high-speed flowfield visualization. This paper covers the test objectives, facility, models and instrumentation, and planned test matrix.

*Aerospace Technologist, Atmospheric Flight & Entry Systems Branch, AIAA Associate Fellow, karl.t.edquist@nasa.gov.

Nomenclature

Symbols

A_{e}	nozzle exit area	in^2
A_{ref}	aerodynamic reference area = projected heatshield frontal area	in^2
A_{t}	nozzle throat area	in^2
C_{T}	vacuum thrust coefficient = $T/\bar{q}A_{\mathrm{ref}}$	
L/D	aerodynamic lift-to-drag ratio	
M_{e}	nozzle exit Mach number	
M_∞	freestream Mach number	
p_{c}	nozzle total pressure	$psia$
p_{e}	nozzle exit static pressure	$psia$
$\bar{q}$	dynamic pressure, $\frac{1}{2}\rho_\infty V_\infty^2$	lb_f/ft^2
R_n	nozzle exit radial location	in
R_b	heatshield radius	in
Re_∞	tunnel Reynolds number	$1/ft$
T	thrust	lb_f
T_{c}	nozzle total temperature	$^\circ F$
T_0	tunnel total temperature	$^\circ F$
V_∞	freestream velocity	m/s
α	angle of attack	deg
ϕ	roll angle	deg
ρ_∞	freestream density	kg/m^3
θ_{cant}	angle between nozzle axis and model longitudinal axis	deg

Acronyms

AI	aerodynamic interference
CFD	computational fluid dynamics
EDL	entry, descent, and landing
HIAD	Hypersonic Inflatable Aerodynamic Decelerator
HPA	high pressure air
NASA	National Aeronautics and Space Administration
PSP	pressure-sensitive paint
SRP	supersonic retropropulsion
LUPWT	Langley Unitary Plan Wind Tunnel

I. Introduction

Over the past decade plus, NASA studies of human-scale Mars entry, descent, and landing (EDL) have concluded that new technologies are needed to enhance or enable delivering payloads to Mars that are much larger than is currently possible.[1–7] One of the enabling technologies is the use of retrorockets, starting at supersonic conditions, in place of a parachute. All studies show that powered descent beginning at supersonic conditions, or supersonic retropropulsion (SRP), is an enabling Mars descent technology for payloads larger than approximately five metric tons. Supersonic parachutes have been used for all of NASA's successful scientific robotic missions to Mars, but they are not scalable for human exploration payloads (approximately 20 metric tons). The largest payload to land on Mars, the Perseverance rover, had a total mass of approximately one metric ton. Powered flight has been successfully executed at Mars subsonic conditions, but it has never been needed at supersonic speeds. The jet interactions between the exhaust plumes and surrounding flowfield result in aerodynamic interference (AI) forces and moments imparted on the entry vehicle that are different from normal unpowered aerodynamics. The uncertainties in powered descent AI on entry vehicle stability, control, and aeroheating are not well understood within the aerosciences community. Thus, there is low confidence in using unvalidated computational fluid dynamics (CFD) methods to predict the aerodynamic and aeroheating loads on Mars powered descent vehicles. CFD uncertainties must be investigated in much more detail than they have been to date, given how significantly they will factor into the overall EDL risk and future mission success for landing humans on Mars.

The current NASA Mars entry system concepts are shown in Figure 1. The reference vehicles are identified by the aerodynamic lift-to-drag ratio (L/D) that they can generate during the hypersonic unpowered entry phase of EDL. The first reference vehicle (Low-L/D) is based on a Hypersonic Inflatable Aerodynamic Decelerator (HIAD) aeroshell that can generate lift-to-drag ratios similar to what the rigid Mars robotic aeroshells can generate (0.24 for the Mars Science Laboratory aeroshell at an angle of attack of about 16 degrees). The second reference vehicle (Mid-L/D) is based on a more slender rigid aeroshell that has body flaps and can generate a higher lift-to-drag ratio (0.54 at a hypersonic trim angle of attack of 55 degrees). Both vehicles have been analyzed assuming a total of eight liquid oxygen and methane (LO_2/CH_4) gas generator cycle engines, each producing approximately 100 kN of thrust, in order to execute a powered descent phase that ends in landing within 50 meters of the target site.[5]

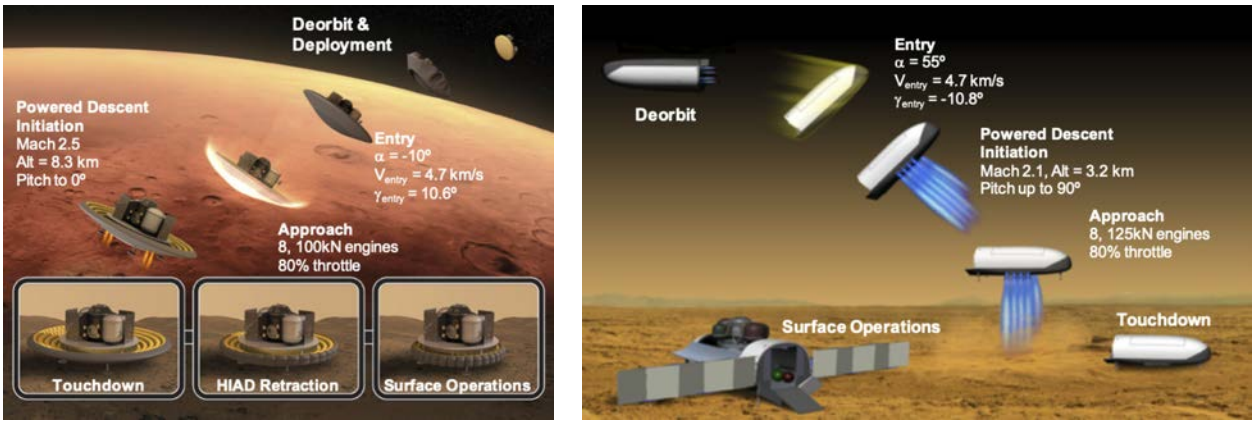

(a) Low-L/D (16.4-meter inflatable aeroshell diameter)

(b) Mid-L/D (22-meter rigid aeroshell length)

Figure 1. Concepts for human Mars entry systems.[7]

Wind tunnel testing, flight testing, and CFD analysis all will play a critical role in advancing powered descent aerosciences. A previous project was used to complete two sub-scale SRP wind tunnel tests[8,9] and companion flowfield analyses[10–12] that showed promising results in the ability of CFD to capture the primary SRP flowfield features. Figure 2 shows example results from a SRP test in the Langley Unitary Plan Wind Tunnel (LUPWT) in 2010. The figure shows instantaneous snapshots of a high-speed schlieren video and a CFD solution for a single-nozzle model with high-pressure air (HPA) jets. Comparisons of general flowfield

structure, discrete pressures on the model surface, and dynamic frequencies gave confidence in the ability of CFD to capture the key features of a relatively simple retropropulsion flowfield. However, AI forces and moments were not measured in the test and the model geometries were not based on current flight-scale concepts. A subsequent project was focused on comparing CFD analysis to one of SpaceX's Falcon 9 first stage return flights that used SRP to decelerate the vehicle.[13–15] This effort greatly advanced the knowledge base for generating large grids and running retropropulsion CFD cases on very large domains with a wide range of length scales. Despite differences in geometry and engine configuration compared to current NASA Mars concepts, the Falcon 9 flight data provided a valuable opportunity to compare Navier-Stokes codes against flight data at Mars-relevant conditions. The CFD results were consistent with the available flight data, both of which showed that the total drag force was dominated by the engine thrust during powered descent. This is in contrast to more recent CFD calculations that show non-negligible aerodynamic drag for NASA Mars concepts, due to the Mars vehicles having significant aerodynamic surface area exposed during powered descent and the engine nozzle exit pressures being similar to ambient conditions.[16]

(a) Schlieren

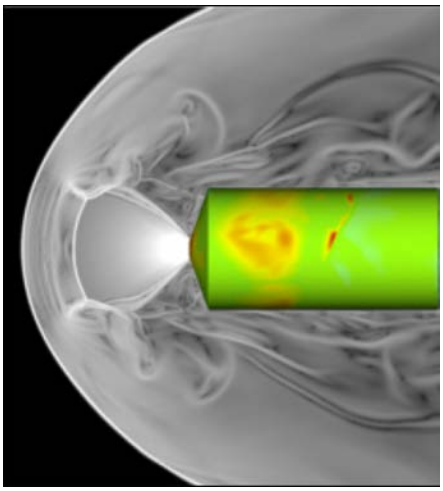

(b) Overflow CFD solution

Figure 2. Schlieren image (a) and Overflow CFD prediction (b) of a single-nozzle SRP model tested in the LUPWT in 2010.[11] Black vertical bars in the schlieren image are bars in the tunnel test section window.

A new SRP test has been designed for the LUPWT, with improvements in model geometries and data products. Portions of the wind tunnel models are scaled versions of the current Low-L/D and Mid-L/D reference vehicles. The outer molds lines and sample engine configurations for both full-scale vehicles are shown in Figs. 3 and 4. Other configurations have also been explored for the Low-L/D reference vehicle with the engines at different locations on the heatshield.[16] Figure 5 shows sample reference trajectories for both vehicles, including transition to powered flight at supersonic conditions.

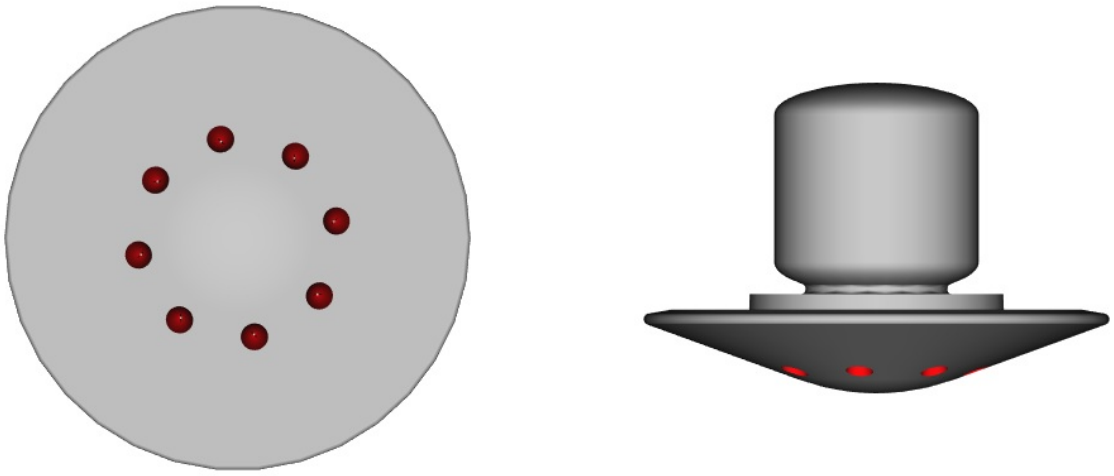

(a) Front view[14] (b) Side view[14]

Figure 3. Low-L/D Mars powered descent vehicle geometry (16.4-meter maximum diameter, evenly spaced engines shown).

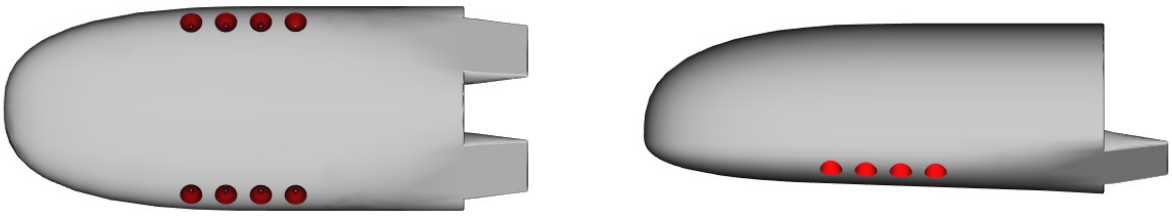

(a) Bottom view[14] (b) Side view[14]

Figure 4. Mid-L/D Mars powered descent vehicle geometry (22-meter total length).

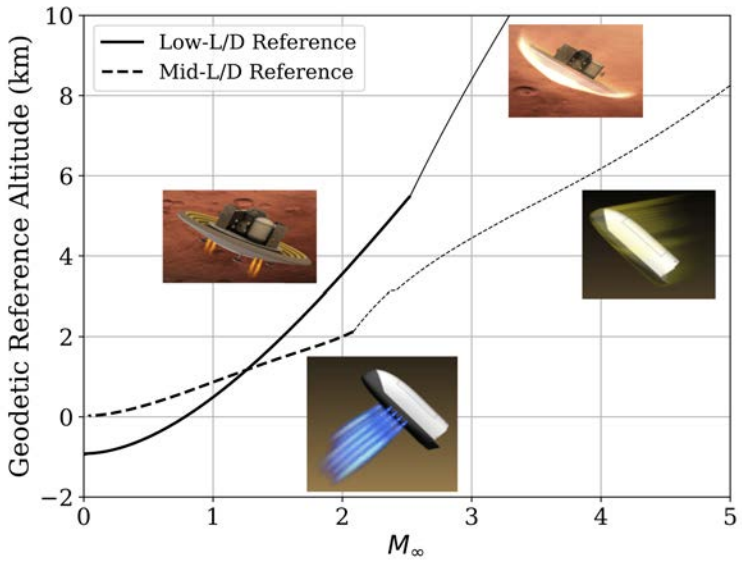

Figure 5. Mars flight reference trajectories. Thicker lines indicate powered descent.

The planned wind tunnel test was designed to address some of the limitations of past ground test data, and will provide a richer SRP data set against which to calibrate CFD models. The test itself is part of a larger NASA program[17] that seeks to evaluate the capabilities of CFD flow solvers to accurately calculate complex flowfields, including SRP. A previous paper[18] provided an initial overview of the planned test campaign and CFD analysis to date. This paper and a companion paper[19] provide updates on the test preparations and CFD analysis. Other aspects of the test campaign include additional pre-test CFD analysis details,[20,21] an experimental plume visualization seeding method,[22] and a custom six-component force and moment balance[23] developed for the test. The following sections describe the test objectives, wind tunnel facility, model designs and instrumentation, and test matrix parameters. Future publications will follow after the completion of the test and will include detailed results and uncertainty analysis, direct comparisons between the test data and CFD results, and an overall assessment of CFD uncertainties for SRP in a wind tunnel environment.

II. Test Objectives

The main objective of the planned test is to produce high-quality quantitative SRP data in a wind tunnel environment by using test articles and conditions that are as relevant to Mars flight conditions as is possible and within constraints of the budget, schedule, and facility. Starting with the model design, the main objective was to fabricate sub-scale versions of current Low-L/D and Mid-L/D Mars reference powered descent vehicles, at a size suitable for testing in the LUPWT. With those models, the primary goal is to explore the effects of different simulated engine nozzle parameters (nozzle location, number, pointing direction, size, area ratio, and thrust) and tunnel/model conditions (Mach number, model attitude) on the measured data. Each model configuration is to be tested across a range of facility and scaling parameter conditions: freestream Mach number (M_∞), angle of attack (α), roll angle (ϕ), and engine scaling parameters (primarily thrust coefficient, C_T). Measurements are to include direct aerodynamic forces and moments from the heatshield, steady-state and high-frequency discrete surface pressures on the external model surfaces, and global steady-state heatshield surface pressure using pressure-sensitive paint. A new seeding method will be attempted that uses oil droplets injected into the model flow path in order to visualize and measure the exhaust plumes. The end goal of the test is to quantify the uncertainties of CFD methods for SRP in a supersonic wind tunnel environment.[19]

III. Test Facility

The test will be conducted in the NASA Langley Research Center Unitary Plan Wind Tunnel, which is a closed-circuit continuous-flow pressure tunnel with two test sections that each have a nominal 4-feet square cross section. The tunnel consists of a 100,000 horsepower compressor, a dry air supply and evacuation system, a cooling system, and paths that circulate air through either of the two test sections (see Figure 6). The Mach number ranges are approximately 1.50 to 2.86 in test section 1 and 2.30 to 4.63 in test section 2. The SRP test will be conducted in test section 2 (see Figure 7), the same section that was used for a 2010 SRP test. The tunnel stagnation pressure can be varied up to a maximum of 100 psia in test section 2. The Mach number is controlled using an asymmetric sliding-block nozzle, which is used to select the nozzle-throat to test-section area ratio. A re-characterization of the tunnel was recently completed, which quantified non-uniform flow in the test section, with varying Mach number and non-zero flow angularity.[24–26] This information will be used to define inflow conditions for CFD analysis of the SRP models with tunnel walls included.

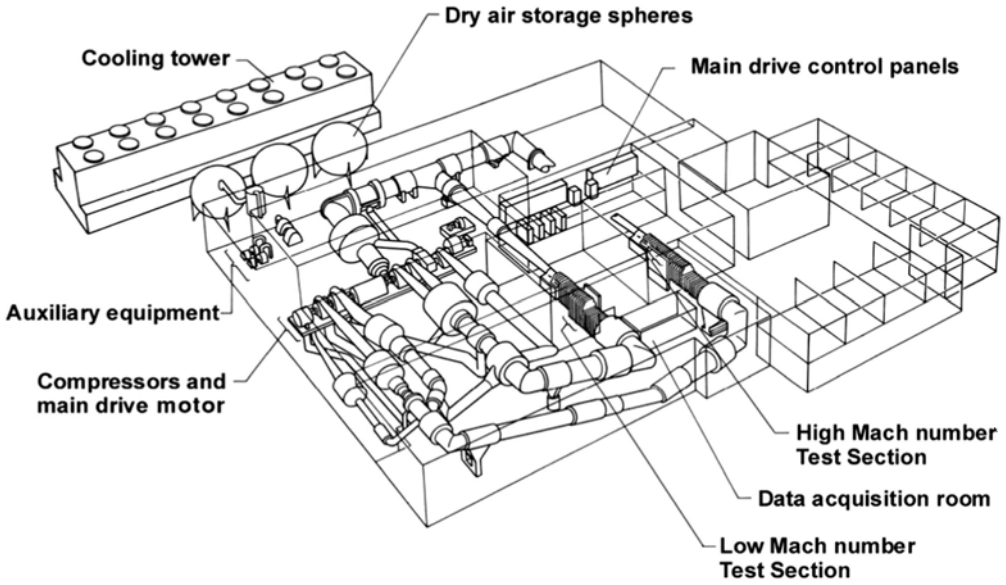

Figure 6. NASA Langley Unitary Plan Wind Tunnel complex.[8]

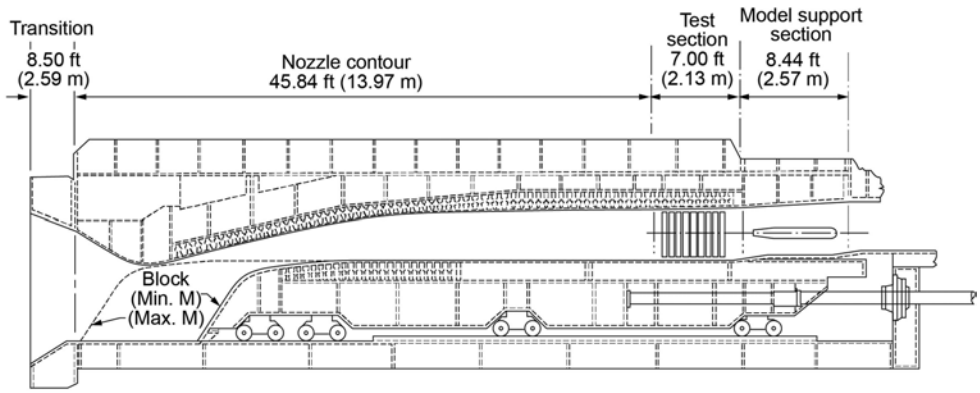

(a) Overview

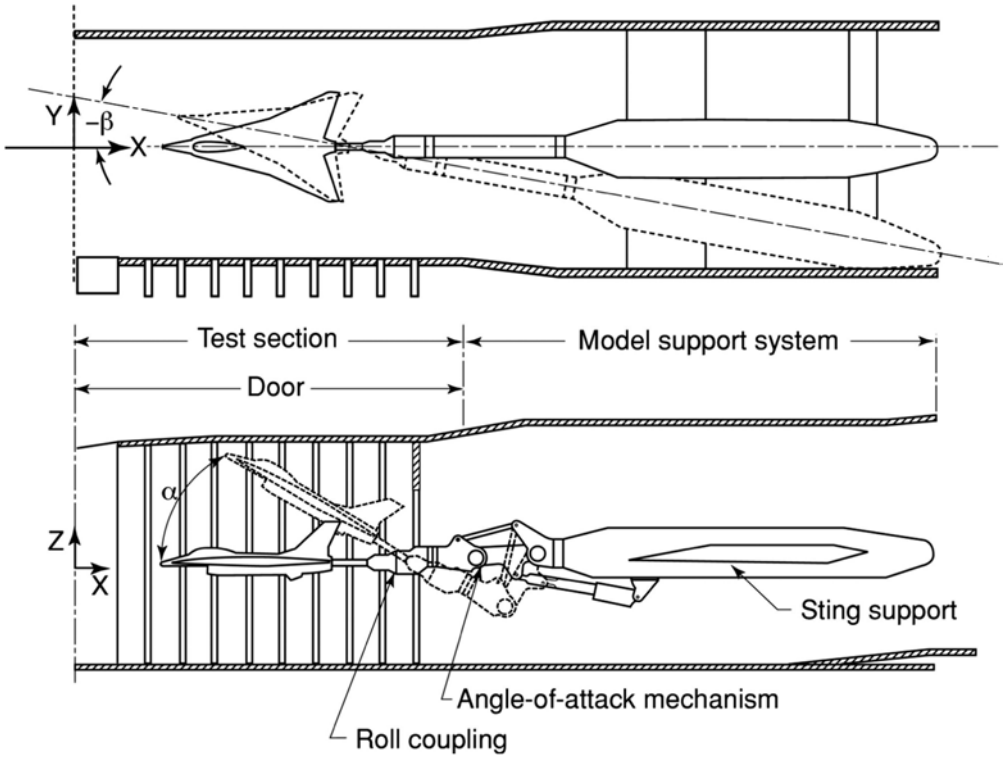

(b) Model support system

Figure 7. NASA Langley Unitary Plan Wind Tunnel (test section 2).[8]

The test section envelope of Mach number and dynamic pressure is shown in Figure 8. Also shown are the 2010 SRP test points and the two flight reference trajectories, with portions of the unpowered (thin lines) and powered (thick lines) segments for each reference vehicle. Neither trajectory's Mach number and dynamic pressure enters the tunnel's envelope, which is typical when comparing Mars conditions to wind tunnel environments.

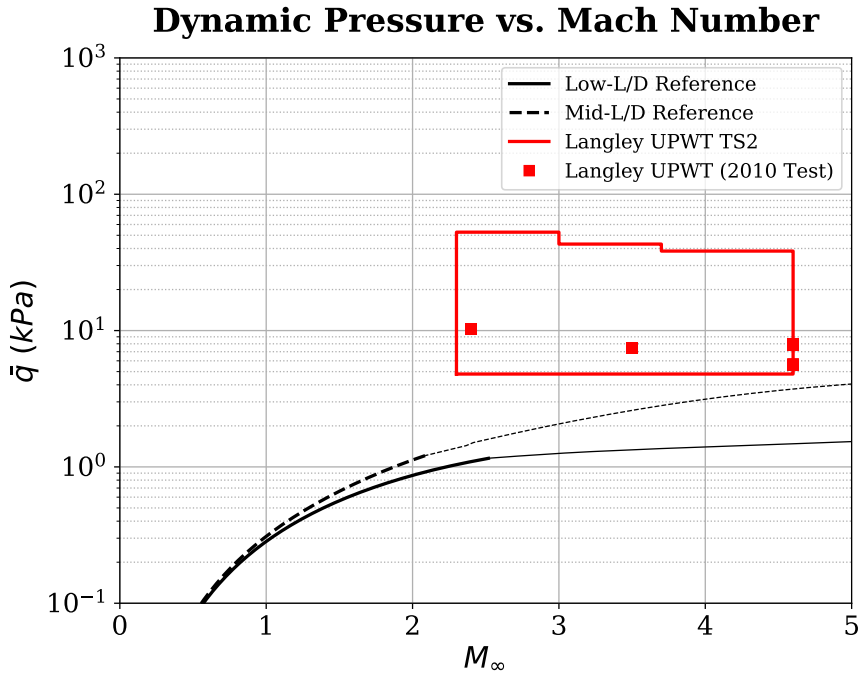

Figure 8. Flight reference trajectories compared to UPWT test section 2 Mach number and dynamic pressure envelope. Thicker lines indicate powered descent.

Table 1 summarizes three LUPWT nominal conditions that are planned for the test campaign and have been used for CFD calculations to date. The test section re-characterization was accomplished using nineteen five-hole probes mounted to a rake that was swept through the test section envelope (Figure 9). The measurements confirmed non-uniform flow in the test section and the results will be used to support overall test uncertainties. CFD analysis of the tunnel test section also was completed[26] and is used in the CFD analysis of the retropropulsion models.[19]

Table 1. Planned LUPWT test conditions.

Condition	M_∞	T_0 ($^\circ F$)	Re_∞/ft	$\bar{q}$ (lb_f/ft^2)
5	2.386	125	1	210.34
20	3.477	125	1	153.22
35	4.568	150	1.5	167.41

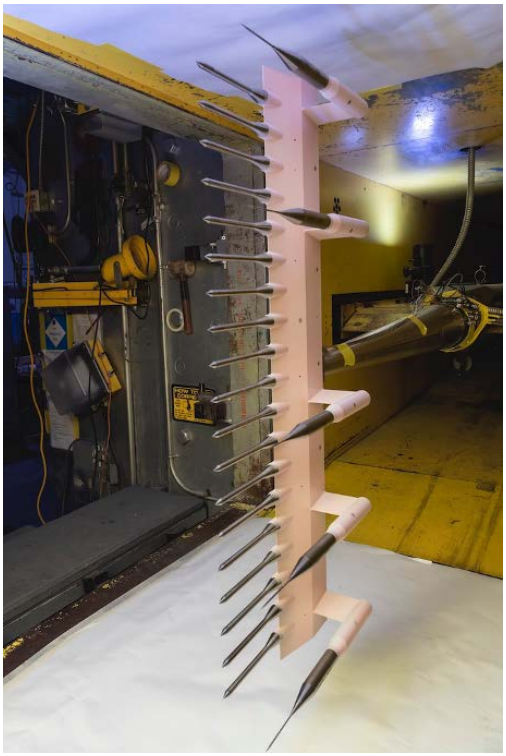

Figure 9. Flow survey rake used for test section re-characterization.[24,25]

IV. Wind Tunnel Models

The primary goal of the wind tunnel model design effort was to make the models as relevant to current human-scale Mars flight reference vehicles as possible. The wind tunnel environment itself is different from powered flight conditions at Mars in number of ways, including the freestream gas (air in the tunnel versus CO_2 at Mars), the Mach and Reynolds numbers, and the plume gases (cold air in the tunnel versus hot combustion products in flight). However, there are a few aspects of the model design that can be controlled to make the test closer to flight. The first is the model heatshield outer mold lines, which will be geometrically scaled from the flight geometries. Second, the simulated engine nozzle exit locations for some models will be placed on the heatshields at the same radial locations that previously were modeled at flight conditions.[16] Also, some of the Low-L/D models, as well as the single Mid-L/D model, will have nozzle exit areas that are the same, relative to the heatshield area, as the set of available flight reference vehicles. This approach for scaling the model heatshield geometries and nozzles makes the current test campaign more relevant for Mars powered flight compared to previous tests. However, there are several scaling parameters that cannot be matched with air as the plume gas.

The three main aspects of Mars powered flight that are significantly different in a wind tunnel test are the thermodynamic properties of the plume gas (ratio of specific heats, molecular weight), the plume gas temperature, and the nozzle exit-to-throat area ratio. Whereas the flight reference vehicles assume 177:1 exit-to-throat area ratio nozzles blowing hot combustion products in front of the vehicle, some concessions in the nozzle geometry and plume gas modeling must be made in the wind tunnel model design. First, an inert gas must be used in the LUPWT in place of real engines, which do not exist nor are they allowed in the tunnel. HPA is already available in the facility and will be used as the exhaust simulant, but it cannot be heated above about 250°F, which is well below the combustion product gas temperature in a flight engine. For the proposed flight engines, the combustion product ratio of specific heats is about 1.28 versus 1.4 for air. Finally, since the HPA cannot be heated significantly, the model nozzle area ratios must be significantly reduced in order to avoid multi-phase air flow due to low temperatures in the expanded plumes. The baseline models will have 4:1 area ratio nozzles, which is the same ratio that was used in the 2010 test campaign.

Using air, the nozzle exit Mach number is 2.94 based on isentropic nozzle relations. One of the Low-L/D models will have 11:1 nozzles, which give an exit Mach number of 4. However, the expanded plume gas temperatures will reach lower temperatures in front of the model and may lead to liquefaction.

The Low-L/D and Mid-L/D models are shown in Figure 11 with the external geometry and the internal flow path for the HPA, which enters the sting at a 90-degree angle. The model sizes are based on past experience with blowing models in the LUPWT. The instrument housing and sting will be common between the two models and the remaining components are tailored to each model. The main part of the two model geometries that is scaled from flight is the front side of the heatshield. The external geometries elsewhere were designed to provide enough internal volume for the instrumentation and HPA flow path.

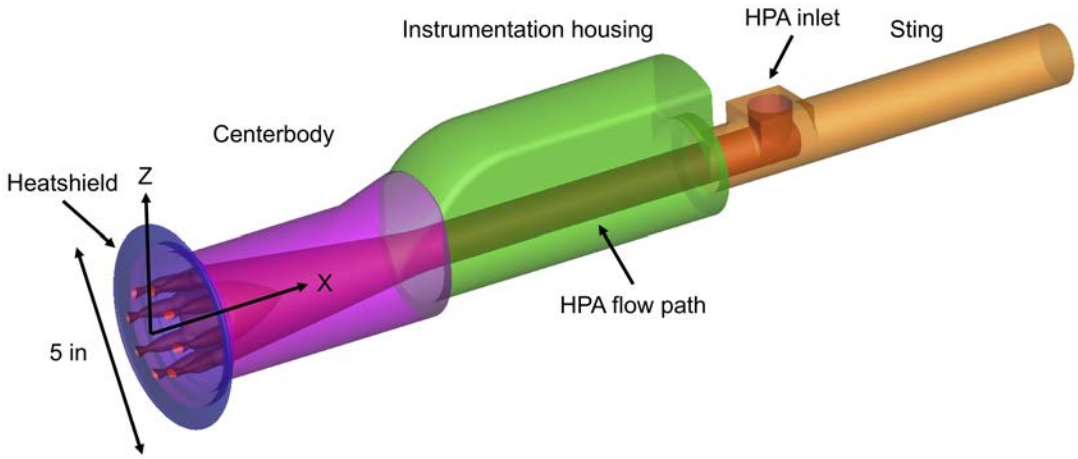

(a) Low-L/D

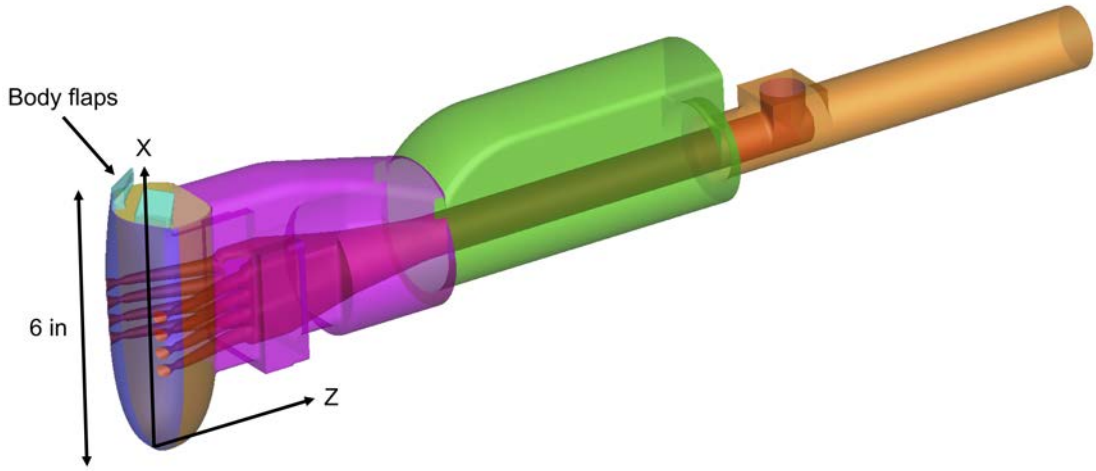

(b) Mid-L/D

Figure 10. Low-L/D (a) and Mid-L/D (b) model external geometries and HPA flow paths.

Figure 11 shows front views of the two model variations: Low-L/D model with interchangeable nozzle inserts (1A through 1F) and Mid-L/D model with a single nozzle configuration (2A). The CFD analysis that has been completed to date at Mars flight conditions, as well as intuition, suggests that there are a few key nozzle parameters that will affect the plume interference characteristics and hence the magnitude of AI forces and moments measured in the wind tunnel. The Low-L/D model will be used to explore some of these key parameters by using interchangeable nozzle inserts (see Table 2). Only a single set of nozzles will be used in the Mid-L/D model.

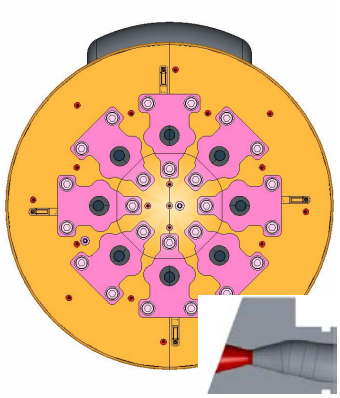

(a) 1A (A_e/A_t=4, θ_{cant}=0°, R_n/R_b=0.434)

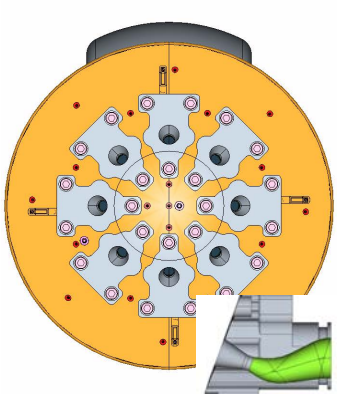

(b) 1B (A_e/A_t=4, θ_{cant}=20°, R_n/R_b=0.434)

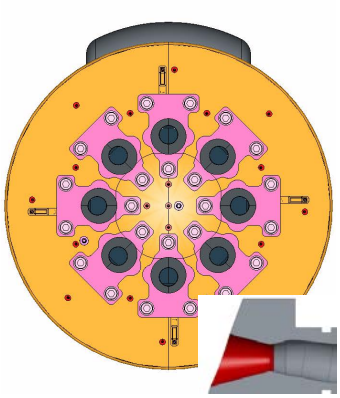

(c) 1C (A_e/A_t=4, θ_{cant}=0°, R_n/R_b=0.434)

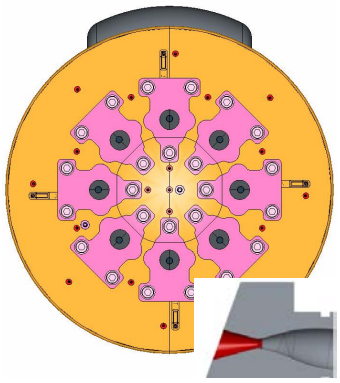

(d) 1D (A_e/A_t=11, θ_{cant}=0°, R_n/R_b=0.434)

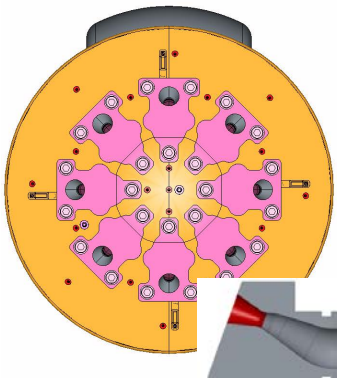

(e) 1E (A_e/A_t=4, θ_{cant}=20°, R_n/R_b=0.6)

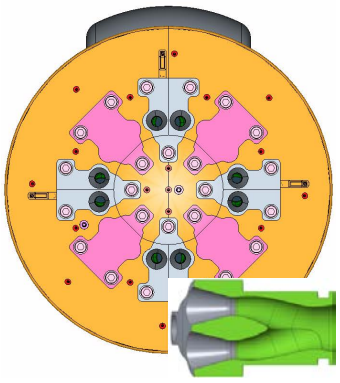

(f) 1F (A_e/A_t=4, θ_{cant}=5°, R_n/R_b=0.434)

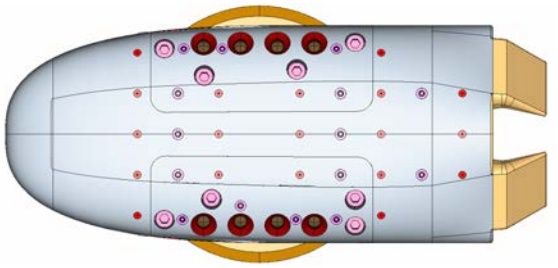

(g) 2A (A_e/A_t=4, θ_{cant}=10°)

Figure 11. Wind tunnel models with a common heatshield and interchangeable nozzle inserts for the Low-L/D model (1A through 1F). Red circles are locations of steady-state pressure measurements. Pink and gray circles are locations of high-frequency pressure measurements.

The key nozzle parameters for both models are shown in Table 2: nozzle radial location on the heatshield (R_n/R_b), cant angle (θ_{cant}), nozzle total exit-to-heatshield area ratio ($\sum A_e/A_{ref}$), nozzle exit-to-throat area ratio (A_e/A_t), and nozzle exit Mach number from compressible flow theory (M_e).

Figure 12 shows the model 1A design with the HPA flow path visible. The flow path was designed to accommodate a single HPA stream that delivers the same plenum conditions to all nozzles at the same time. The HPA flow path contours were designed to reduce turning angles, which keeps total pressure and temperature losses to an acceptable level. All nozzles will have 15-degree conical convergent and divergent sections, with a short straight section for the throat. The nozzle exits are scarfed to follow the heatshield surface contour. Figure 13 shows the model 1A design mounted to sting and tunnel support hardware.

Table 2. Model parameters compared to flight reference vehicles.

Geometry	R_n/R_b	θ_{cant} (deg)	$\sum A_e/A_{\text{ref}}$	A_e/A_t	M_e
Low-L/D (Flight)	0.434	5	0.062	177	5.6
1A	0.434	0	0.062	4	2.94
1B	0.434	20	0.062	4	2.94
1C	0.434	0	0.112	4	2.94
1D	0.434	0	0.062	11	4.03
1E	0.6	20	0.062	4	2.94
1F	0.434 (paired)	5	0.062	4	2.94
Mid-L/D (Flight)	N/A	10	0.051	177	5.6
2A	Same as flight	10	0.051	4	2.94

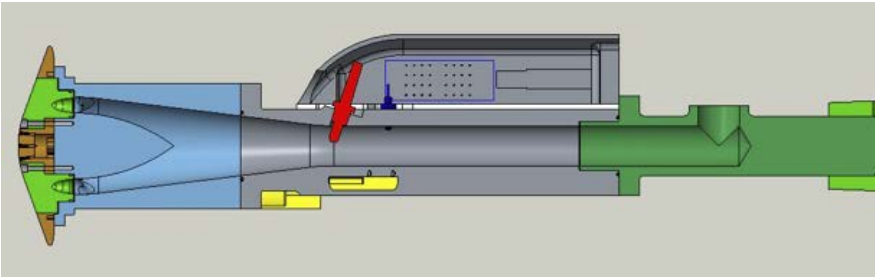

Figure 12. Low-L/D model design with HPA internal flow path.

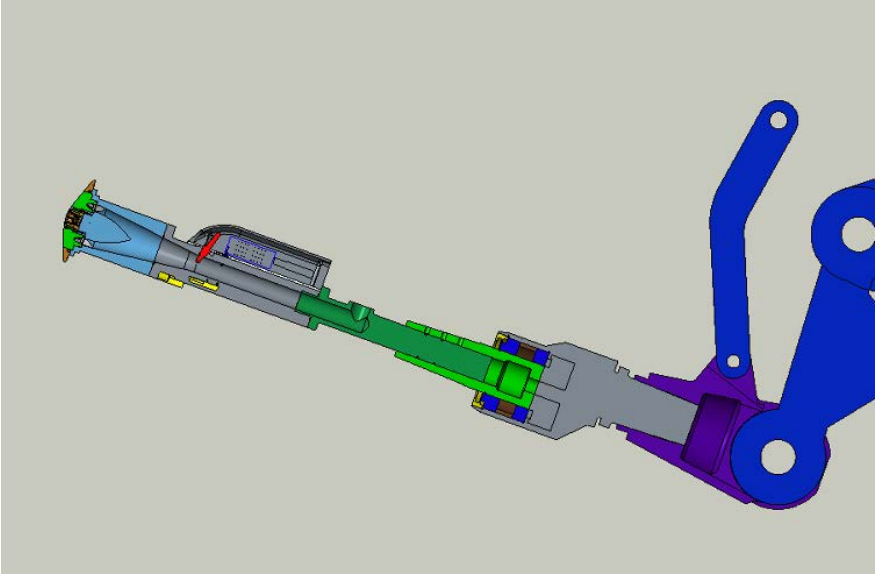

Figure 13. Low-L/D model design mounted to sting and support hardware.

Figure 14 shows pictures of fabricated model hardware taken during inspection. A fit check of all parts was completed successfully, including all nozzle inserts and pressure instrumentation connections.

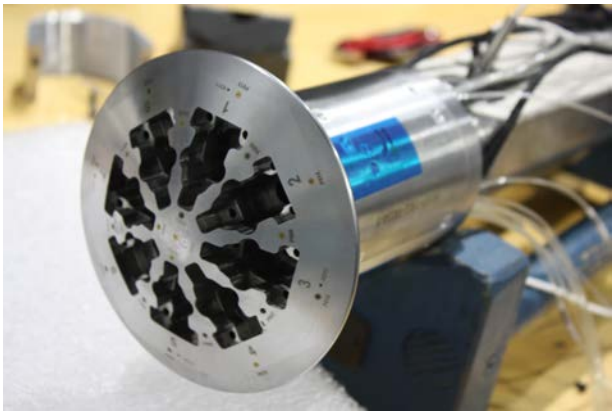

(a) Low-L/D heatshield with nozzle inserts removed

(b) Low-L/D heatshield with nozzle inserts

(c) Low-L/D heatshield with main plenum and instrument housing

(d) Mid-L/D heatshield with nozzle inserts removed

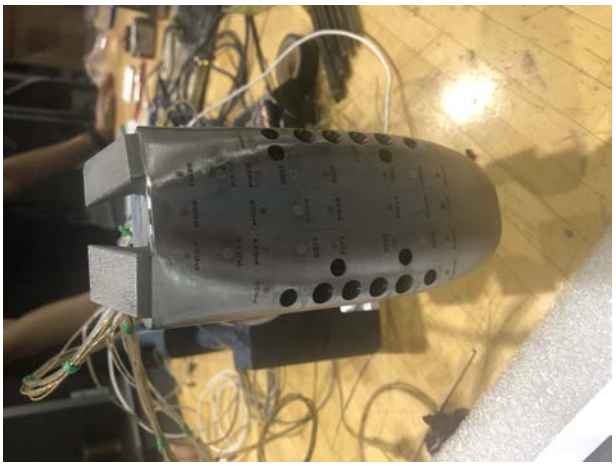

(e) Mid-L/D heatshield with nozzle inserts

(f) Mid-L/D heatshield with main plenum and instrument housing

Figure 14. Model hardware.

V. Instrumentation

The upcoming test will incorporate some of the same types of measurements that were last used in the 2010 UPWT SRP test,[8] in addition to new measurement techniques aimed specifically at the SRP problem. Table 3 summarizes pressure and temperature measurements to be taken. As was done in 2010, static and unsteady pressure will be measured at discrete locations on the external model surfaces and inside the flow path. The external measurements will include static pressure taps and Kulites on the heatshield front and rear surfaces where the most important interactions between the nozzle plumes and external flow are expected to occur; these measurements will be directly compared to unsteady and time-averaged CFD results. Pressure measurements inside the model flow path will provide a status of the blowing HPA flowing through the models. Finally, pressure measurements on the tunnel upper wall may be used to assess the possible impact of the retropropulsion flowfield on the tunnel freestream conditions, such as excessive blockage or unstart. Figure 15 shows the model pressure and temperature measurement locations and Figure 16 shows pressure tap locations on the tunnel upper wall.

Table 3. Model and tunnel pressure and temperature measurements with number of locations.

Location	Steady discrete pressure	Unsteady discrete pressure	Steady PSP	Discrete Temperature
Model HPA flow path	0	2	N/A	1
Low-L/D model heatshield (front)	20	6	Yes	0
Low-L/D model heatshield (rear)	2	4	No	0
Mid-L/D model heatshield	20	15	Yes	0
Model centerbody (side)	29	4	No	0
Tunnel nozzle section (upper wall)	80	0	N/A	N/A
Tunnel test section (upper wall)	21	0	N/A	N/A
Tunnel model support section (upper wall)	18	0	N/A	N/A

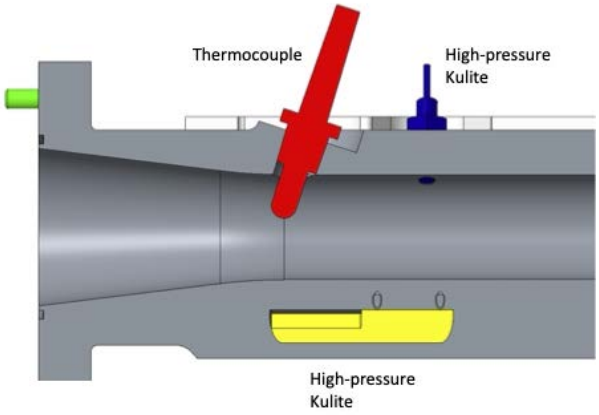

(a) HPA flow path

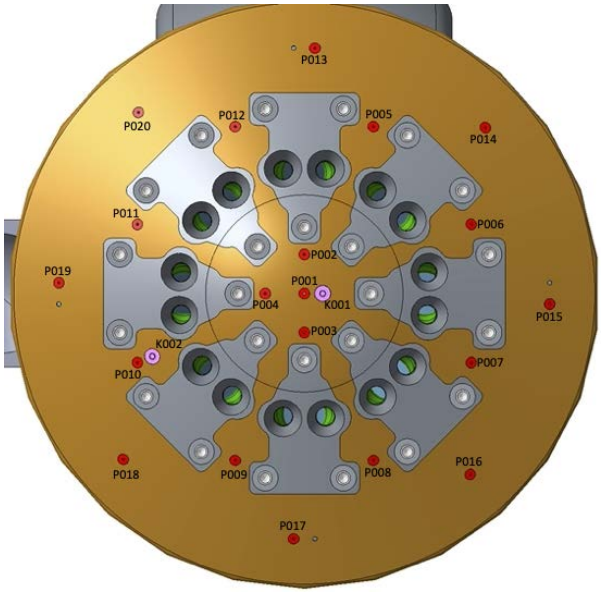

(b) Low-L/D heatshield (front)

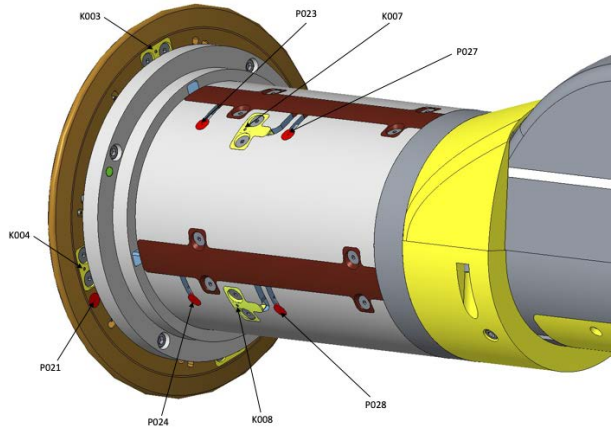

(c) Low-L/D heatshield (rear) and centerbody

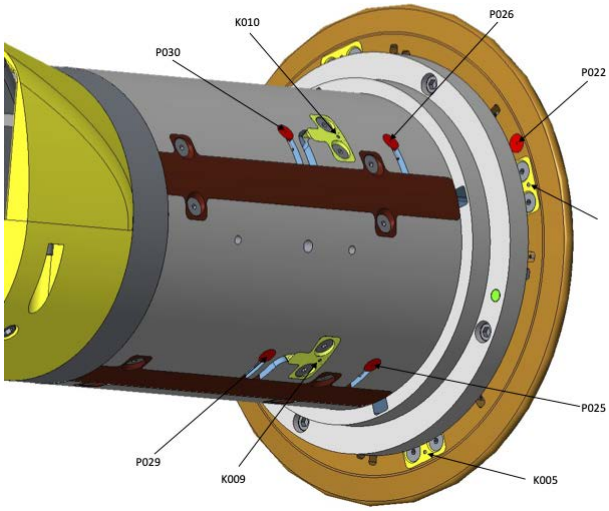

(d) Low-L/D heatshield (rear) and centerbody

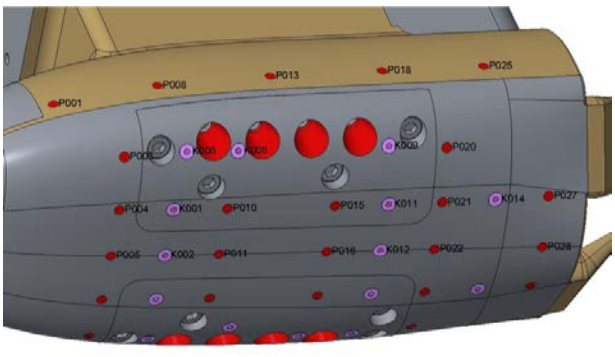

(e) Mid-L/D heatshield (front)

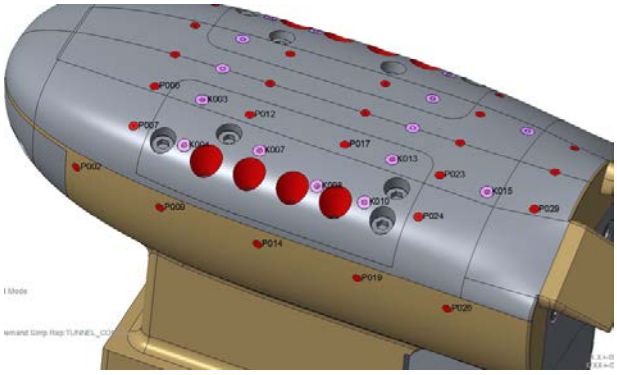

(f) Mid-L/D heatshield (front)

Figure 15. Model discrete pressure ("P" = steady, "K" = unsteady) and temperature measurements.

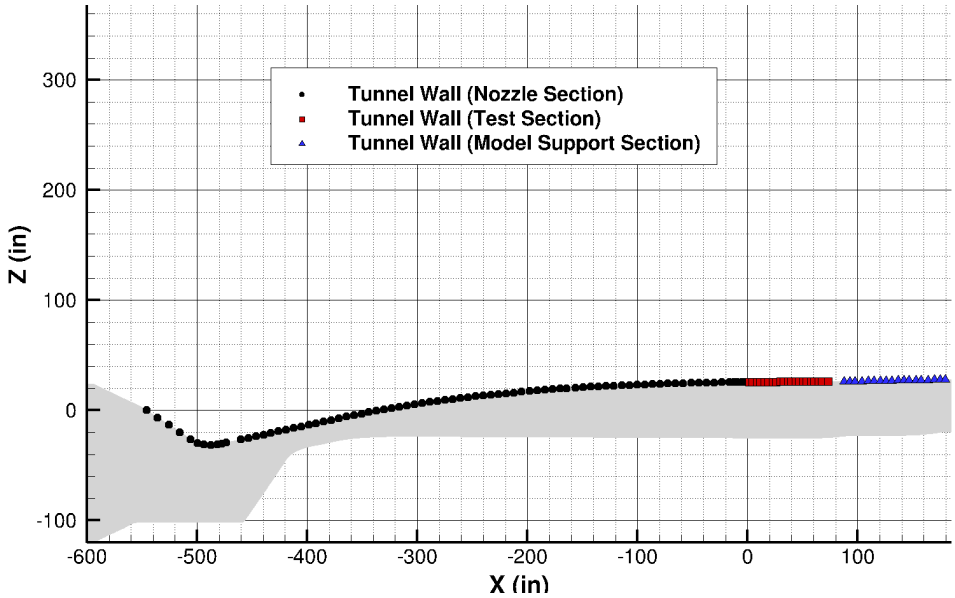

Figure 16. Tunnel pressure measurements.

Pressure-sensitive paint (PSP) will be applied to the front sides of both model heatshields in order to provide steady-state pressure distributions that can be directly compared to time-averaged CFD pressures. A high-speed digital camera will be used to record schlieren video in order to capture the dynamic interactions between the nozzle plumes, model, and tunnel flow. Frame rates between 5,000 and 10,000 frames per second were used for the 2010 test; a similar rate is expected to suffice for the upcoming test. The high-speed video will provide quantitative data, such as observed unsteady frequencies and bow shock standoff distances, as well as a qualitative picture of the overall aerodynamic-propulsive interaction flowfield.

Delays in the facility and testing schedule allowed time for a new nozzle plume seeding device[22] and flow-through force and moment balance[23] to be designed and built after the models were fabricated. The seeding method shown in Figure 17 is based on a Venturi contraction that draws oil particles into the HPA flow path and out the nozzles, where a laser sheet is used to observe the particles. The seeding method is considered experimental for the upcoming test. The force and moment balance was designed specifically to be retro-fitted to the models in order to measure six-component forces and moments during testing. Figure 18 shows the balance design and hardware. The balance is designed to optimize accuracy in the axial force measurement, which is of high interest for powered flight. A shield was designed so that the balance will measure forces and moments generated by the heatshield only. The flow adapters are designed to direct the flow into and out of the balance section with manageable total pressure loss. Thrust measurements will be made on the balance with the tunnel off to provide curves of thrust versus HPA total pressure. The measured thrust will be subtracted from the measurements that are taken during the test in order to isolate the aerodynamic contributions from the model heatshield. The balance will provide the first known measurement of six-component forces and moments in a retropropulsion wind tunnel test. Direct comparisons between the balance measurements and CFD solvers will be the primary metric for assessing predictive modeling capabilities.

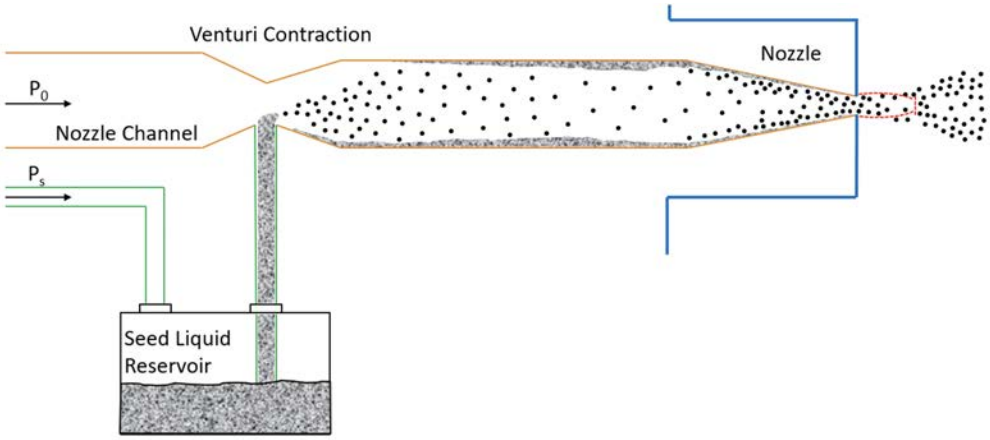

Figure 17. Plume seeding concept.

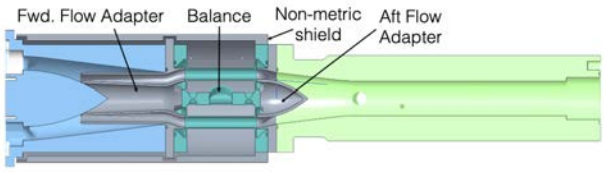

(a) Balance design with shield and flow adapter

(b) Balance

(c) Balance and shield

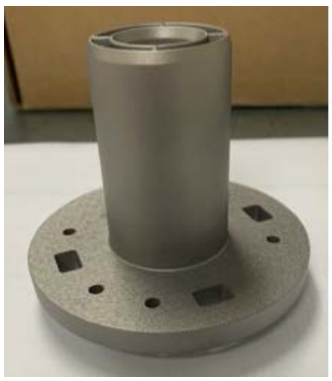

(d) Flow adapters

Figure 18. Six-component force and moment balance.

VI. Test Matrix

The test matrix for each model is designed to investigate plume/flowfield interactions as a function of the main model and facility parameters: nozzle configuration, nozzle thrust, model angle of attack and roll angle, and tunnel Mach number. Each model will be tested with plugged nozzles in order to measure surface pressures and aerodynamic forces and moments and to compare to unpowered CFD cases and to previously

measured values for similar geometries. For blowing cases, the strategy will be to test each model for a range of HPA total pressures over a range of model angles of attack and roll angles at each tunnel condition. The range of HPA total pressure used for each model will be selected to follow a specific schedule of thrust coefficients that is common across all blowing model configurations. The thrust coefficient upper bound for each model will be based on whether tunnel interference or blockage is observed.

The priorities for the test are as follows. First, the Low-L/D model will be given higher priority because it is believed to be the more likely full-scale vehicle and because the model was designed to observe the effects of various nozzle parameters. Second, the lowest Mach number (2.386 for tunnel condition 5) will be prioritized in the test matrix because it is closest to the predicted in-flight Mach number at the start of SRP. If the high-speed video and PSP methods do not permit simultaneous operation, due to insufficient room for equipment next to the test section window, the video will be given higher priority. Finally, the force and moment balance measurements will be given priority over all other measurements due to the importance of having those measurements for CFD assessment. The plume seeding technique likely will be done at the end of the test campaign due to its experimental nature and the unknown effects of the seeding oil on the model and tunnel.

Table 4. Test matrix parameters.

Parameter	Low-L/D Model	Mid-L/D Model
Configurations	1 (plugged), 1A, 1B, 1C, 1D, 1E, 1F	2 (plugged), 2A
Tunnel conditions	5, 20, 35	5, 20, 35
HPA p_c (psia)	up to 1500	up to 1500
HPA T_c ($^\circ F$)	up to 250	up to 250
Model α (deg)	-10 to 20	80 to 110
Model ϕ (deg)	0, 22.5 or 45	0

Figure 19 shows example test points at three different tunnel Mach numbers for model 1A for a range of HPA total pressures (p_c). During the test at each model angle of attack and roll angle, the HPA pressure will be adjusted to select a range of common thrust coefficients in order to explore AI versus that scaling parameter. The nozzle exit pressure divided by the freestream stagnation pressure ($p_e/p_{0,2}$), another common plume scaling parameter, is an indication of how the nozzle plume will behave in terms of overall dimensions and dynamic behavior. The plan for the test is to investigate each model for both over-expanded conditions, where the nozzle exit pressure is lower than local ambient pressure in the shock layer, and under-expanded conditions where the exit pressure is higher. The boundary between over- and under-expanded nozzles is not well understood even for simple single-nozzle configurations, and the physics are more complicated for multi-engine configurations and non-zero angles of attack.[27] Coincidentally, the Low-L/D flight reference vehicle with 177:1 engine nozzles has a pressure ratio of unity near the start of powered descent. Finally, because the nozzle gas (air) and area ratios for the wind tunnel models are different than a real rocket engine, flight values for C_T and $p_e/p_{0,2}$ cannot be matched at the same time in the wind tunnel environment. This reason, along with others discussed previously, means that the wind tunnel test data cannot be treated as a true sub-scale version of flight.

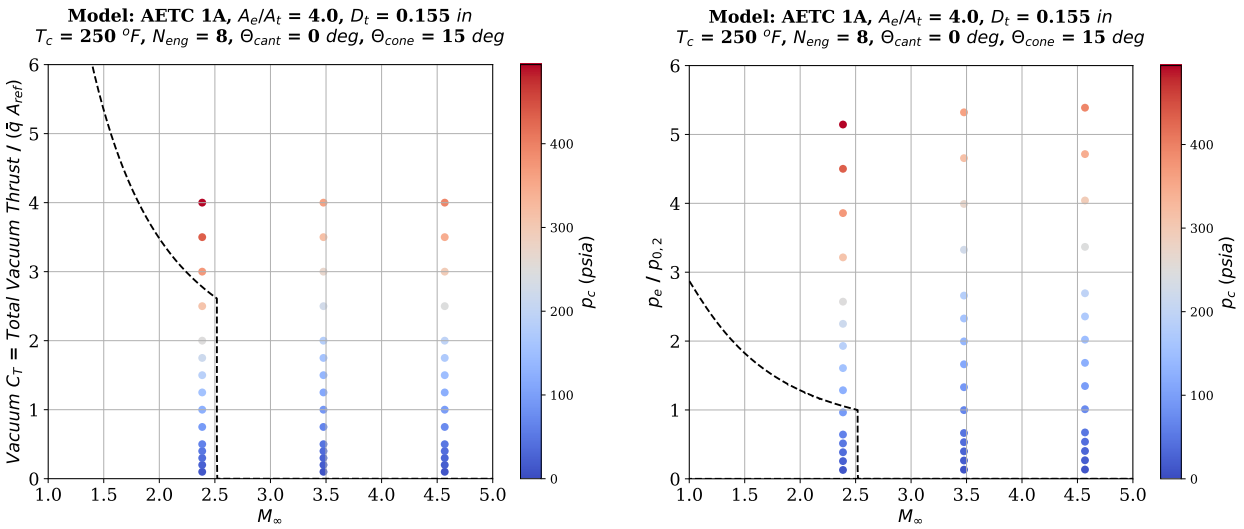

(a) Thrust coefficient

(b) Ratio of nozzle exit pressure to freestream post-shock stagnation pressure

Figure 19. Sample Low-L/D model 1A thrust coefficients (a) and nozzle exit pressure ratios (b) for a range of nozzle total pressures (using one-dimensional isentropic nozzle equations). Reference powered flight trajectories with 177:1 engine nozzles are shown as black dashed lines.

VII. Summary and Conclusions

A sub-scale test will be run in the NASA Langley Research Center Unitary Plan Wind Tunnel test section 2 in order to investigate aerodynamic interference effects due to simulated retrorocket nozzle plumes at supersonic freestream conditions (supersonic retropropulsion). The main test objective is to collect data on wind tunnel models that are derived from current NASA human-scale Mars powered descent vehicles, using air as the simulated engine gas. Two wind tunnel models were designed and fabricated to be geometrically-scaled versions of the current flight reference vehicles: a blunt sphere-cone vehicle and a more slender geometry. Both models accommodate up to eight blowing nozzles, like the flight reference vehicles, and the blunt heatshield has interchangeable nozzle inserts that will allow different nozzle parameters to be investigated for their effects on aerodynamic interference: location on heatshield, pointing direction, exit area divided by heatshield area, and exit area divided by throat area. The test data will consist of six-component forces and moments using a custom flow-through balance, high-speed schlieren video, steady and high-frequency discrete surface pressures, global surface pressure using pressure-sensitive paint, and internal flow path pressure and temperature. An experimental method for visualizing the nozzle plumes was developed and will be part of the test campaign. The post-test analysis and documentation will include extensive uncertainty quantification of both the data and parallel computational flowfield simulations at tunnel conditions.

Acknowledgments

The wind tunnel model design, fabrication, and facility time are funded by NASA's Aerosciences Evaluation and Test Capability program office under the Aeronautics Research Mission Directorate.

Nicholas Marino and Donald Morr of Millennium Engineering and Integration Services completed the model designs for fabrication.

References

[1]Braun, R. D., and Manning, R. M., "Mars Exploration Entry, Descent, and Landing Challenges," *Journal of Spacecraft and Rockets*, Vol. 44, No. 2, 2007, pp. 310–323.

[2]Dwyer-Ciancolo, A. M., et al, "Entry, Descent and Landing Systems Analysis Study: Phase 1 Report," NASA TM 216720, National Aeronautics and Space Administration, July 2010.

[3]Dwyer-Ciancolo, A. M., et al, "Entry, Descent and Landing Systems Analysis Study: Phase 2 Report on Exploration Feed-Forward Systems," NASA TM 217055, National Aeronautics and Space Administration, February 2011.

[4]Edquist, K. T., Korzun, A. M., Dyakonov, A. A., Studak, J. W., Kipp, D. M., and Dupzyk, I. C., "Development of Supersonic Retropropulsion for Future Mars Entry, Descent, and Landing Systems," *Journal of Spacecraft and Rockets*, Vol. 51, No. 3, 2014, pp. 650–663.

[5]Cianciolo, A. D., and Polsgrove, T. T., "Human Mars Entry, Descent, and Landing Architecture Study Overview," AIAA Paper 2016-5494, September 2016.

[6]Cianciolo, A. D., and Polsgrove, T. T., "Human Mars Entry, Descent and Landing Architecture Study: Phase 2 Summary," AIAA Paper 2018-5191, September 2018.

[7]Cianciolo, A. D., Korzun, A., Edquist, K., Samareh, J., Sostaric, R., Calderon, D., and Garcia, J. A., "Human Mars Entry, Descent and Landing Architecture Study: Phase 3 Summary," AIAA Paper 2020-1509, January 2020.

[8]Berry, S. A., Rhode, M. R., and Edquist, K. T., "Supersonic Retropropulsion Validation Experiment in the NASA Langley Unitary Plan Wind Tunnel," *Journal of Spacecraft and Rockets*, Vol. 51, No. 3, 2014, pp. 664–679.

[9]Berry, S. A., Rhode, M. R., and Edquist, K. T., "Supersonic Retropropulsion Experimental Results from NASA Ames 9×7 Foot Supersonic Wind Tunnel," *Journal of Spacecraft and Rockets*, Vol. 51, No. 3, 2014, pp. 724–734.

[10]Zarchi, K. A., Schauerhamer, D. G., Kleb, W. L., Carlson, J.-R., and Edquist, K. T., "Analysis of Navier-Stokes Codes Applied to Supersonic Retropropulsion Wind–Tunnel Test," *Journal of Spacecraft and Rockets*, Vol. 51, No. 3, 2014, pp. 680–692.

[11]Schauerhamer, D. G. Zarchi, K. A., Kleb, W. L. Carlson, J.-R., and Edquist, K. T., "Supersonic Retropropulsion Computational Fluid Dynamics Validation with Langley 4x4 Foot Test Data," *Journal of Spacecraft and Rockets*, Vol. 51, No. 3, 2014, pp. 693–714.

[12]Schauerhamer, D. G. Zarchi, K. A., Kleb, W. L., and Edquist, K. T., "Supersonic Retropropulsion Computational-Fluid-Dynamics Validation with Ames 9x7 Foot Test Data," *Journal of Spacecraft and Rockets*, Vol. 51, No. 3, 2014, pp. 735–749.

[13]Braun, R. D., Sforzo, B., and Campbell, C., "Advancing Supersonic Retropropulsion Using Mars-Relevant Flight Data: An Overview," AIAA Paper 2017-5292, September 2017.

[14]Edquist, K. T., et al, "Comparison of Navier-Stokes Flow Solvers to Falcon 9 Supersonic Retropropulsion Flight Data," AIAA Paper 2017-5296, September 2017.

[15]Sforzo, B. and Braun, R. D., "Feasibility of Supersonic Retropropulsion Based on Assessment of Mars-Relevant Flight Data," AIAA Paper 2017-5295, September 2017.

[16]Korzun, A., Canabal, F., Tang, C., Childs, R., Van Norman, J., Tynis, J., and Bibb, K., "Powered Descent Aerodynamics for Low and Mid Lift-to-Drag Human Mars Entry, Descent and Landing Vehicles," AIAA Paper 2020-1510, January 2020.

[17]Ross, J. C., et al, "Evaluation of CFD as a Surrogate for Wind-Tunnel Testing for Mach 2.4 to 4.6 - Project Overview," AIAA Paper 2021-2961, August 2021.

[18]Edquist, K. T., Korzun, A. M., Kleb, B., Hawke, V. M., Rizh, Y. M., Olsen, M. E., Canabal, F., "Model Design and Pre-Test CFD Analysis for a Supersonic Retropropulsion Wind Tunnel Test," AIAA Paper 2020-2230, January 2020.

[19]Edquist, K. T., Alter, S. J., Glass, C. E., Kleb, W. L., Korzun, A. M., Wood, W. A., Childs, R. E., Halstrom, L. D., Matsuno, K. V., and Canabal, F., "Computational Modeling of Mars Retropropulsion Concepts Tested in the Langley Unitary Plan Wind Tunnel," AIAA Paper 2022-XXXX, January 2022.

[20]Halstrom, L. D., Pulliam, T. H., Childs, R. E., and Stremel, P. M., "OVERFLOW Analysis of Supersonic Retropropulsion Testing on a Blunt Mars Entry Vehicle Concept," AIAA Paper 2022-XXXX, January 2022.

[21]Matsuno, K. V., Childs, R. E., Stremel, P. M., Garcia, J. A., and Pulliam, T. H., "OVERFLOW Analysis of Supersonic Retropropulsion Testing on the CobraMRV Mars Entry Vehicle Concept," AIAA Paper 2022-XXXX, January 2022.

[22]Acharya, A. S., Lowe, K. Todd, Danehy, P. M., Edquist, K. T., Burns, R. A., and Pham, H. T., "Seeding Method for Velocimetry and Visualization of Supersonic Retropropulsion Nozzle Plumes," AIAA Paper 2022-XXXX, January 2022.

[23]Burns, D. E., Parker, P. A., Cagle, C. M., Hawke, V. M., Tor, K. G., and Kleb, B., "A New Flow-Through Wind Tunnel Balance for Retropropulsion Testing," AIAA Paper 2022-XXXX, January 2022.

[24]Rhode, M. N., et al, "Flow Characterization of the NASA Langley Unitary Plan Wind Tunnel, Test Section 2: Experimental Results," Aiaa presentation, August 2021.

[25]Hubbard, E. P., and Houlden, H. P., "Evaluation of CFD as a Surrogate for Wind-Tunnel Testing: Experimental Uncertainty Quantification for the UPWT Flow Survey Test," AIAA Paper 2021-2962, August 2021.

[26]Childs, R. E., et al, "Flow Characterization of the NASA Langley Unitary Plan Wind Tunnel, Test Section 2: Computational Results," AIAA Paper 2021-2963, August 2021.

[27]Korzun, A. M., and Cassel, L. A., "Scaling and Similitude in Single Nozzle Supersonic Retropropulsion Aerodynamics Interference," AIAA Paper 2020-0039, January 2020.